

Generalized Griffith criterion for dynamic fracture and the stability of crack motion at high velocities

M. Adda-Bedia,¹ R. Arias,² M. Ben Amar,¹ F. Lund²

¹Laboratoire de Physique Statistique de l'École Normale Supérieure, 24 rue Lhomond, F-75231 Paris Cedex 05, France

²Departamento de Física, Facultad de Ciencias Físicas y Matemáticas, Universidad de Chile, Casilla 487-3, Santiago, Chile

(Received 18 November 1998)

We use Eshelby's energy momentum tensor of dynamic elasticity to compute the forces acting on a moving crack front in a three-dimensional elastic solid [Philos. Mag. **42**, 1401 (1951)]. The crack front is allowed to be any curve in three dimensions, but its curvature is assumed small enough so that near the front the dynamics is locally governed by two-dimensional physics. In this case the component of the elastic force on the crack front that is tangent to the front vanishes. However, both the other components, parallel and perpendicular to the direction of motion, do not vanish. We propose that the dynamics of cracks that are allowed to deviate from straight line motion is governed by a vector equation that reflects a balance of elastic forces with dissipative forces at the crack tip, and a phenomenological model for those dissipative forces is advanced. Under certain assumptions for the parameters that characterize the model for the dissipative forces, we find a second order dynamic instability for the crack trajectory. This is signaled by the existence of a critical velocity V_c such that for velocities $V < V_c$ the motion is governed by $K_{II} = 0$, while for $V > V_c$ it is governed by $K_{II} \neq 0$. This result provides a qualitative explanation for some experimental results associated with dynamic fracture instabilities in thin brittle plates. When deviations from straight line motion are suppressed, the usual equation of straight line crack motion based on a Griffiths-like criterion is recovered. [S1063-651X(99)12408-5]

PACS number(s): 46.05.+b, 62.20.Mk, 46.50.+a, 81.40.Np

I. INTRODUCTION

Experiments carried out over the past ten years with thin plates of glass and plexiglass have uncovered a wealth of phenomena associated with dynamic fracture [1–5]. When the crack velocity V exceeds a critical speed V_c , a dynamic instability occurs: The velocity of the crack starts to oscillate, the crack surface becomes rough, microcracks branch out of the main crack, acoustic emission from the crack increases, velocity oscillations are amplified, and a pattern more or less correlated with the velocity oscillations appears on the fracture surface. One recent experiment [6] has focused on the role played by microcracks, while another [7] has shown that even a modest amount of acoustic energy may induce a significant change in the velocity of a running crack. Those measurements that have been performed both in glass and plexiglass indicate that, after proper normalization, those effects are the same in both materials. A remarkable fact given their very different microstructure.

Standard theoretical tools to understand crack dynamics are based on dynamic elasticity in two dimensions [8]. This theoretical framework predicts that a crack in tension will accelerate smoothly, asymptotically approaching the Rayleigh wave velocity. For quite some time, however, there have been experimental results at variance with conclusions based on this analysis [9]. The experiments mentioned in the previous paragraph are sufficiently accurate to place quantitative bounds on deviations from the smooth, straight trajectory that a simple minded two-dimensional analysis yields.

Over the last several years, there have been a number of attempts to explain the complexity of the dynamics of the crack tip. Studies based on a continuum approach to the crack problem have been made, and it has been suggested

that the crack instabilities are due to three-dimensional effects [10,11], or to the effect of large deformations near the crack tip, requiring a nonlinear analysis [12]. Another point of view has emphasized that complete dynamical models of deformation and decohesion at crack tips [13,14] are necessary in order to understand the experimental observations. It has also been argued [15] that conventional continuum theories are inherently inadequate to describe crack dynamics, and lattice models have accordingly been proposed and solved (see also Ref. [16]). Finally, a number of studies have been undertaken using large scale molecular dynamics simulations [17–19]. In spite of this considerable effort, it does not seem unfair to say that there are well established experimental observations that, to date, have defied theoretical understanding.

Current theory of brittle fracture mechanics is essentially based on the determination of a characteristic quantity called the energy release rate G [8], or rate of decrease of elastodynamic energy per unit crack advance. Within purely elastic assumptions, the crack must grow in such a way that G is always equal to a newly defined quantity Γ , the dynamic fracture energy of the material [8,20]. The parameter Γ includes the energy associated with the creation of a new crack surface, as well as the energy associated with whatever nonlinear processes take place on a microscopic scale very near the crack tip. However, this is only one condition, and it is not enough to completely determine the crack tip motion that is allowed to deviate from a straight line. Effectively, the generalized Griffith criterion [8,20] is a scalar equation, while crack motion has three degrees of freedom. Therefore, in order to complete the description of crack motion, additional criteria, such as the principle of local symmetry [21,22], have been introduced.

In thermodynamics terms, G is the generalized force con-

jugate to the extension of a crack. There are two ways to compute this quantity. The first of these [23,24] is a global dissipation analysis which recognizes the fact that the fracture of a material sample is thermodynamically, irreversible while the local mechanical behavior of the bulk material may be fully elastic. The second one [25,26] directly involves the computation of the generalized, or configurational, force of a *non-Newtonian* type which acts at the tip of the crack, which is considered as a defect. This is the point of view of the theory of defects, or material inhomogeneities, and material forces on singularities introduced by Eshelby in 1951 [25]. Configurational forces in conjunction with an inequality based on the second law of thermodynamics have been recently used to propose a framework for crack propagation [27,28].

In this paper, we propose an approach based on the full consideration of all components of the configurational force at the crack front. It is found that this force does not necessarily point in the direction of crack propagation, and we propose a generalization of Griffith's approach [20] in order to take this fact into account. Within this framework, we develop a model of forces balance, instead of energy balance. Under minimal assumptions, we show that there exists a critical crack velocity, below which the crack propagates in a direction that keeps a pure opening mode at the tip. Above the critical velocity, this mode of crack propagation is no longer favored, and there appears a dynamic instability. A number of experimental results can thereby be qualitatively understood. A preliminary announcement of these results was presented in Ref. [29].

This paper is organized as follows. In Secs. II and III, we introduce the main theoretical ingredients of our analysis. We review the derivation of the Eshelby energy-momentum tensor [26,30], and we present the balance of energy and field momentum for a moving crack front. This motivates the introduction of the energy flow rate into the crack front and the material forces acting on it. The analysis of these two Sections is valid in three dimensions, and for quite general constitutive relations, including nonlinear stress-strain relations. In Sec. IV, we derive the explicit form of the material forces in a linear isotropic elastodynamic solid. The commonly used equation of motion [8] corresponds to a balance of energy at the crack front. We point out that it also corresponds to the balance of configurational forces in one direction, the direction of motion. In Sec. V, we show that within a Griffith-like approach, it is possible to define a generalized dissipative force at the crack front. Assuming that elastic and dissipative forces acting at the crack front exactly balance, we derive a vector equation of motion. In Sec. VI we show that within our model a second order dynamic instability is possible: above a critical velocity (smaller than the Rayleigh velocity), crack growth with a pure opening mode at the tip becomes unstable with respect to two new possible solutions. Section VII is devoted to the interpretation of some of the experimental results of Refs. [1–5] within the framework of this model. Concluding remarks are offered in Sec. VIII.

II. BALANCES OF ENERGY, LINEAR AND FIELD MOMENTA

In this section we review some concepts of energy and momentum balance in an elastic solid [26,30]. We will use a

Lagrangian description, with variables associated to a reference, or undistorted, configuration. The volume and boundary of this reference configuration are denoted by V and S , respectively, and their points are described in terms of a Cartesian basis \vec{E}_i ($i=1,2,3$) as $\vec{X}=X_i\vec{E}_i$. The dynamics of the solid is given by the evolution of those points as a function of time. Their position is given by the current, or distorted, configuration

$$\vec{x}=\vec{\chi}(\vec{X},t)=\vec{X}+\vec{u}(\vec{X},t), \quad (1)$$

with $\vec{u}(\vec{X},t)$ the displacement field. The local balance of the linear momentum reads

$$\frac{\partial}{\partial t}(\rho_o(\vec{X})v_i(\vec{X},t))-\frac{\partial p_{ij}}{\partial X_j}(\vec{X},t)=\rho_o(\vec{X})f_i(\vec{X},t), \quad (2)$$

with $v_i(\vec{X},t)=u_{i,t}\equiv\partial u_i/\partial t$ the particle velocity, p_{ij} the nominal stress tensor, $\rho_o(\vec{X})$ the mass density per unit volume, and $\vec{f}(\vec{X},t)$ the body force per unit mass. They are all defined with respect to the reference configuration. The nominal stress tensor p_{ij} is given by

$$p_{ij}(\vec{X},t)=\frac{\partial}{\partial u_{i,j}}W(u_{k,l},\vec{X},t), \quad (3)$$

with W the strain energy per unit initial volume, and $u_{i,j}\equiv\partial u_i/\partial X_j$. The equation of motion [Eq. (2)], together with boundary conditions on the surface S ,

$$\mathcal{T}_i=p_{ij}n_j,$$

where \mathcal{T}_i is the traction exerted by external loads on the surface that points in the direction n_i , can also be obtained as the extremum of the action

$$\begin{aligned} \mathcal{A} &= \int_{t_i}^{t_f} dt \int_V d\vec{X} [\mathcal{L}(u_{i,t}, u_{i,j}, X_i, t) + \rho_o(\vec{X})f_i(\vec{X}, t)u_i(\vec{X}, t)] \\ &+ \int_{t_i}^{t_f} dt \int_S dS \mathcal{T}_i(\vec{X}, t)u_i(\vec{X}, t), \end{aligned} \quad (4)$$

with respect to variations of $\vec{u}(\vec{X},t)$. This procedure leads to the following Euler-Lagrange equations, representing linear momentum balance:

$$\frac{\partial}{\partial t} \left(\frac{\partial \mathcal{L}}{\partial u_{i,t}} \right) + \frac{\partial}{\partial X_j} \left(\frac{\partial \mathcal{L}}{\partial u_{i,j}} \right) = \rho_o f_i. \quad (5)$$

This equation is equivalent with Eq. (2) if the Lagrangian density \mathcal{L} is defined as

$$\mathcal{L}(u_{i,t}, u_{i,j}, X_i, t) \equiv T(u_{i,t}, X_i) - W(u_{i,j}, X_i, t), \quad (6)$$

where $T = \frac{1}{2}\rho_o(\vec{X})\vec{v}^2$ is the kinetic energy density.

Multiplying Eq. (2) by v_i and rearranging, the following equation of energy balance results:

$$\frac{\partial}{\partial t} (T + W) + \frac{\partial}{\partial X_j} (-p_{ij}v_i) = \rho_o f_i v_i - \frac{\partial \mathcal{L}}{\partial t} \Big|_{\text{expl}}, \quad (7)$$

where the subscript *expl* designs the explicit material derivative of the Lagrangian density. Likewise, multiplying Eq. (2) by $\partial u_i / \partial X_k$ one can obtain the following equation of field momentum balance:

$$\begin{aligned} \frac{\partial}{\partial t} \left(\rho_o v_i \frac{\partial u_i}{\partial X_k} \right) + \frac{\partial}{\partial X_j} \left(-\mathcal{L} \delta_{kj} - p_{ij} \frac{\partial u_i}{\partial X_k} \right) \\ = \rho_o f_i \frac{\partial u_i}{\partial X_k} - \frac{\partial \mathcal{L}}{\partial X_k} \Big|_{\text{expl}}, \end{aligned} \quad (8)$$

where the field momentum density is defined as $-\rho_o v_i \partial u_i / \partial X_k$ [26]. Note that this quantity is dimensionally a density of linear momentum, i.e., mass density times velocity, but it is not the ‘‘physical’’ momentum $\rho_o v_i$. Indeed, the field momentum per unit volume of the reference configuration, also known as quasimomentum or pseudomomentum, is the difference between the linear momentum $\rho_o v_k$ and the canonical momentum $\rho_o v_k + \rho_o v_i \partial u_i / \partial X_k$ [26,30].

Equations (7) and (8) in the absence of body forces ($f_i = 0$), and in an homogeneous and stationary medium ($\partial \mathcal{L} / \partial X_k |_{\text{expl}} = 0$, $\partial \mathcal{L} / \partial t |_{\text{expl}} = 0$) represent energy and field momentum conservation. In the absence of body forces, the energy and field momentum balance can be written in the form

$$\frac{\partial T_{\mu\nu}}{\partial X_\nu} = - \frac{\partial \mathcal{L}}{\partial X_\mu} \Big|_{\text{expl}}, \quad (9)$$

with $\mu, \nu = 0, 1, 2, \text{ and } 3$ and $X_0 \equiv t$. Note that, although we use four-dimensional notation for convenience, Greek indices do not label the four components of vectors. The components of the Eshelby energy-momentum tensor $T_{\mu\nu}$ are [26]

$$\begin{aligned} T_{00} &= T + W, & T_{0i} &= -p_{ji} v_j, \\ T_{i0} &= \rho_o v_j \frac{\partial u_j}{\partial X_i}, & T_{ij} &= -\mathcal{L} \delta_{ij} - p_{kj} \frac{\partial u_k}{\partial X_i}, \end{aligned} \quad (10)$$

with T_{00} the energy density, T_{0i} the energy density flux, $-T_{i0}$ the field momentum density, and $-T_{ij}$ the field momentum density flux. These formulas can be encapsulated in the following compact form:

$$T_{\mu\nu} = -\mathcal{L} \delta_{\mu\nu} + \frac{\partial \mathcal{L}}{\partial u_{i,\nu}} u_{i,\mu}. \quad (11)$$

Note that throughout this section it has been assumed that the solid is elastic, in the sense that stresses can be obtained as gradients of a potential energy function W [Eq. (3)]. Nothing has been assumed, however, about the functional dependence of W upon strain. In particular, the solid need not be linearly elastic.

Consider now the motion of a given domain $\mathcal{B}(t)$ of the reference frame, bounded by a surface $\partial \mathcal{B}(t)$, within an homogeneous elastic body of volume \mathcal{V} , itself bounded by an external surface \mathcal{S} . The domain \mathcal{B} is in motion with a velocity \vec{V} , measured in the reference, or undistorted, frame. We look for the energy and field momentum flow into this domain. It is allowed for this domain to contain an inhomogeneity, or a singularity of the elastic fields, or to intersect the external surface. This last possibility will be used in Sec. III,

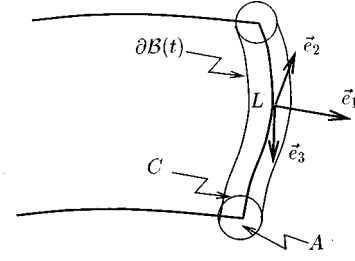


FIG. 1. Schematic representation of a crack surface. A local orthonormal basis \vec{e}_i ($i=1, 2, \text{ and } 3$) is associated with the crack front. The front itself is a curve whose parameter is L . Arguments involving energy and momentum balance involve a cylindrical volume around the crack front. This cylinder is bounded by a surface $\partial \mathcal{B}(t)$ of cross section A , whose rim is given by a curve C .

in which $\mathcal{B}(t)$ will surround a crack tip. Integrating Eq. (9) within the volume \mathcal{V} but excluding the domain \mathcal{B} , and under the assumption that $\partial \mathcal{L} / \partial X_\mu |_{\text{expl}} = 0$ in $\mathcal{V} - \mathcal{B}$, leads to the following equation of energy-momentum balance:

$$\frac{d}{dt} \int_{\mathcal{V} - \mathcal{B}(t)} d\vec{X} T_{\mu 0} = \int_{\mathcal{S}} dS_i T_{\mu i} + \int_{\partial \mathcal{B}(t)} dS_i [T_{\mu i} - V_i T_{\mu 0}]. \quad (12)$$

Since T_{00} is the energy density, we can interpret the $\mu=0$ component of this equation as an equation of field energy balance: the change in elastic energy within the volume $\mathcal{V} - \mathcal{B}$ per unit time is equal to the work performed at the surface \mathcal{S} minus the quantity

$$\mathcal{W} = - \int_{\partial \mathcal{B}(t)} dS_i [T_{0i} - V_i T_{00}], \quad (13)$$

which can thus be identified as the rate of energy flow into the moving domain \mathcal{B} through its boundary $\partial \mathcal{B}$. Similarly, since $-T_{j0}$ is the density of field momentum, taking the $\mu=j$ component of Eq. (12) yields an equation of momentum balance: the change in field momentum within $\mathcal{V} - \mathcal{B}$ is given by the elastic force performed at the surface \mathcal{S} minus the quantity

$$\mathcal{P}_j = \int_{\partial \mathcal{B}(t)} dS_i [T_{ji} - V_i T_{j0}], \quad (14)$$

which can thus be identified as the rate of flow of field momentum into the moving domain \mathcal{B} through its boundary $\partial \mathcal{B}$.

III. ENERGY AND FIELD MOMENTUM BALANCE FOR A MOVING CRACK

We now apply the previous formalism to a three-dimensional solid within which there is a moving crack. The crack front is a line $\vec{R}(L, t)$, with L a Lagrangian coordinate that labels points along the crack front, where elastic fields are singular. The crack front velocity is $\vec{V}(L, t) \equiv \partial \vec{R}(L, t) / \partial t$. We take as the domain \mathcal{B} a thin cylinder surrounding the crack front and the surface $\partial \mathcal{B}(t)$ the surface of this cylinder; it starts on one crack lip, encircles the crack front, and ends on the other crack lip (see Fig. 1). We assume that during crack propagation both the crack surface and the

crack front remain smooth with continuously turning tangents. Otherwise, the local frame at the crack front is ill defined.

The instantaneous rate of energy flow $\mathcal{F}(L,t)$ entering into the region of the crack front per unit of its length [8,23,24] is given by the specialization of Eq. (13) to the case of a thin cylindrical surface just mentioned,

$$\mathcal{F}(L,t) \equiv \frac{d\mathcal{W}}{dL} = - \lim_{C \rightarrow 0} \int_C dC [T_{0i}N_i - V_i T_{00}N_i], \quad (15)$$

where C is a curve that encircles the crack front along the surface of the cylinder $\partial\mathcal{B}(t)$, within a plane locally perpendicular to the crack front (see Fig. 1), and N_i is the unit normal to this curve. The instantaneous rate of flow of field momentum into the region of the crack front can be identified as a configurational force $F_j(L,t)$ acting on it [26,30], whose value is found, from Eq. (14), to be

$$F_j(L,t) \equiv \frac{d\mathcal{P}_j}{dL} = \lim_{C \rightarrow 0} \int_C dC [T_{ji}N_i - V_i T_{j0}N_i]. \quad (16)$$

We emphasize that $\mathcal{F}(L,t)$ and $F_j(L,t)$ are defined *per unit length of the crack front*: the total rate of energy flow and total forces are given by $\mathcal{W} = \int_L dL \mathcal{F}(L,t)$ and $\mathcal{P}_j = \int_L dL F_j(L,t)$, respectively.

Some insight into the nature of the force \vec{F} may be obtained by considering the field momentum balance for the volume *within* $\mathcal{B}(t)$, assuming that elasticity, not necessarily linear and not necessarily homogeneous but obeying the assumptions of Sec. II, holds. Simple integration gives

$$\begin{aligned} \frac{d}{dt} \int_{\mathcal{B}(t)} d\vec{X} (-T_{j0}) &= \int_{\mathcal{B}(t)} d\vec{X} \frac{\partial}{\partial t} (-T_{j0}) \\ &+ \int_{\partial\mathcal{B}(t)} dS_i (-T_{j0}) V_i. \end{aligned} \quad (17)$$

Use of the local field momentum balance [Eq. (9)], and of Eq. (14) for the field momentum flow into the domain $\mathcal{B}(t)$, leads to

$$\frac{d}{dt} \int_{\mathcal{B}(t)} d\vec{X} (-T_{j0}) = \int_{\mathcal{B}(t)} d\vec{X} \left. \frac{\partial \mathcal{L}}{\partial X_j} \right|_{\text{expl}} + \mathcal{P}_j(t). \quad (18)$$

For the actual calculation of these forces and energy flow, we take the displacement field within $\mathcal{B}(t)$ to be of the form

$$u_i = u_i^o(\vec{X} - \vec{R}(L,t), t) + u_i'(\vec{X}, t), \quad (19)$$

with $\partial u_i^o / \partial X_j \gg \partial u_i' / \partial X_j$, and $\partial u_i^o / \partial t \approx -V_j \partial u_i^o / \partial X_j$. To the extent that the dominant contribution \vec{u}^o leads to a divergence of T_{j0} weaker than $|\vec{X} - \vec{R}(L,t)|^{-2}$, the left hand side of Eq. (18) will be zero, and accordingly, per unit length of the crack front the following holds:

$$F_j(L,t) = - \lim_{A \rightarrow 0} \int_A \left. \frac{\partial \mathcal{L}}{\partial X_j} \right|_{\text{expl}} dA, \quad (20)$$

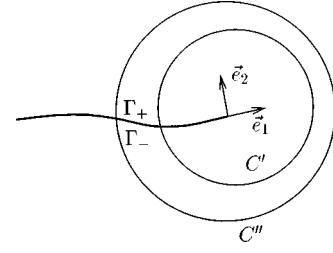


FIG. 2. Two different contours of integration C' and C'' surrounding the crack tip. A closed surface is defined by them, plus two lines Γ_+ and Γ_- along the upper and lower lips of the crack surface that lie between C' and C'' .

with A the cross sectional area of $\mathcal{B}(t)$. This last relation for the material forces $F_j(L,t)$ suggests that they may be balanced by inhomogeneities of the elastic field very near the crack front.

Equations (15) and (16) must be path independent in order to have fundamental significance, and we now show that this is the case. Consider two distinct crack-tip encircling curves C' and C'' , and the closed contour formed by C' and C'' plus two straight segments Γ_+ and Γ_- along the crack faces (Fig. 2). The integrand $I_{\mu i} = T_{\mu i} - V_i T_{\mu 0}$ that appears in Eqs. (15) and (16) for \mathcal{F} and F_i renders a null result when integrated over the closed curve $C' + \Gamma_+ + C'' + \Gamma_-$, provided the displacement field u_i has the near-field asymptotic behavior [Eq. (19)]. This behavior is satisfied by linear elastodynamic fields close to the crack front (see Sec. II). This result is established by applying the divergence theorem to the integral and by incorporating the energy and field momentum balances, Eqs. (7) and (8), with $f_i = 0$ and $\partial \mathcal{L} / \partial X_\nu = 0$. The integration of \mathcal{F} over Γ_\pm is equal to zero. The integration of F_j over Γ_+ is the negative of the integration over Γ_- and leads to a cancellation because, due to the near field behavior [Eq. (19)] $\mathcal{L}_+ = \mathcal{L}_-$, with \mathcal{L}_\pm the Lagrangian evaluated on the segments Γ_\pm , respectively. From this one deduces that, as long as both C' and C'' are close to the tip,

$$\begin{aligned} \mathcal{F} &= - \int_{C'} dS_i I_{0i} = - \int_{C''} dS_i I_{0i}, \\ F_j &= \int_{C'} dS_i I_{ji} = \int_{C''} dS_i I_{ji}. \end{aligned} \quad (21)$$

This proves the independence of the result on the shape of the curve C , as long as it is near the crack front [31].

The force \vec{F} can be related to the energy flow rate \mathcal{F} [23,26,30]. Using the explicit expressions for $T_{\mu\nu}$ from Eq. (10) and the near field behavior $v_i \approx \partial u_i^o / \partial t \approx -V_j \partial u_i^o / \partial X_j$ [see Eq. (19)], a direct substitution into Eqs. (15) and (16) shows that

$$\mathcal{F}(L,t) = V_i(L,t) F_i(L,t). \quad (22)$$

This important result gives a physical interpretation to the force \vec{F} on the crack front; the work done by the force for an infinitesimal advance of the crack front, $\vec{F} \cdot d\vec{R}$, is *equal* to the energy entering the crack front per unit length during that time, $\mathcal{F} dt$.

IV. ENERGY FLOW AND MATERIAL FORCES FOR A GROWING CRACK

We now specialize to the case of elastodynamic crack growth within a linearly elastic material. In this case the strain energy density is $W = p_{ij}u_{i,j}/2$, with $p_{ij} = C_{ijpq}\partial u_p/\partial X_q$, where C_{ijpq} is the elastic constants tensor. We shall assume that derivatives along a direction locally parallel to the crack front are smaller than derivatives along a direction locally perpendicular to it, so that the singular structure of the elastic fields near the crack front is locally two dimensional [32].

Consider a crack front moving under loading in modes I, II (plane strain conditions), and III. Define a local frame \vec{e}_i such that \vec{e}_1 is the local unit vector normal to the crack front along its direction of motion, \vec{e}_3 is the local unit vector tangent to the crack front and $\vec{e}_2 = \vec{e}_3 \wedge \vec{e}_1$ (see Fig. 1). In the vicinity of each point of the crack front, the universal part of the stress and displacement velocity elastic fields are well known to be [8]

$$p_{ij}(r, \theta, t) = \sum_I \frac{K_I(L, t)}{\sqrt{2\pi r}} P_{ij}^I(\theta, V), \quad (23)$$

$$v_i(r, \theta, t) = \sum_I \frac{VK_I(L, t)}{\mu\sqrt{2\pi r}} V_i^I(\theta, V), \quad (24)$$

with (r, θ) polar coordinates in the plane (\vec{e}_1, \vec{e}_2) based on the crack front at the position L . $V = V_\perp(L, t)$ is the local instantaneous velocity of the crack front, normal to itself. $K_I(L, t)$ ($I=I, II, III$) are the stress intensity factors corresponding to the three possible modes of local loading. $P_{ij}^I(\theta, V)$ and $V_i^I(\theta, V)$ are universal angular functions independent of the specific loading conditions and geometry.

As already mentioned, the evaluation of the rate of energy flow \mathcal{F} and the forces F_i is path independent, as long as the path is close to the crack front. Thus, in Eqs. (15) and (16) we chose the curve C as a circle of small radius around the moving crack tip, such that the asymptotic values (23) and (24) hold. Using these values together with the definition (10) yields

$$\frac{1}{V}\mathcal{F}(L, t) \equiv G(L, t) = F_1(L, t), \quad (25)$$

$$F_1(L, t) = \frac{1}{2\mu} [A_I(V)K_I^2 + A_{II}(V)K_{II}^2 + A_{III}(V)K_{III}^2], \quad (26)$$

$$F_2(L, t) = -\frac{1}{2\mu} B(V)K_I K_{II}, \quad (27)$$

$$F_3(L, t) = 0, \quad (28)$$

where μ is the elastic shear modulus. G is the *dynamic energy release rate* per unit length of the crack front [8], and

$$A_I(V) = \frac{a(1-b^2)}{D(V)}, \quad (29)$$

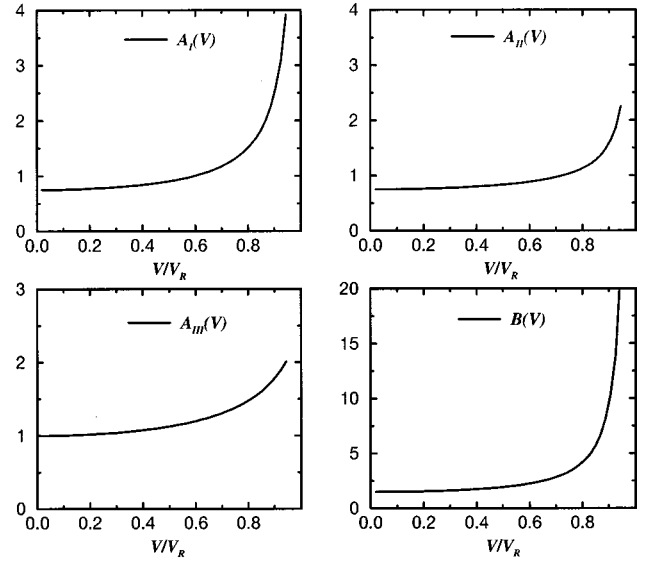


FIG. 3. Universal functions $A_i(V)$ ($i=I, II, III$) and $B(V)$, given by Eqs. (29)–(32), plotted as a function of V/V_R for $C_d = \sqrt{3}C_s$.

$$A_{II}(V) = \frac{b(1-b^2)}{D(V)}, \quad (30)$$

$$A_{III}(V) = \frac{1}{b}, \quad (31)$$

$$B(V) = \frac{4ab(1-b^4)(a-b)}{D(V)^2}, \quad (32)$$

with $a(V) \equiv \sqrt{1 - V^2/C_d^2}$, $b(V) \equiv \sqrt{1 - V^2/C_s^2}$, and $D(V) \equiv 4ab - (1 + b^2)^2$. C_d and C_s are the longitudinal and shear sound velocities, respectively. Note that the Rayleigh velocity of surface waves, V_R , is a solution of $D(V_R) = 0$. The functions $A_i(V)$ and $B(V)$ are also universal in the sense that they do not depend on the details of the applied loading or the configuration of the body being analyzed. They do depend on the local *instantaneous* speed normal to the crack front and on the properties of the material. For low velocities, $V \rightarrow 0$, they have the behaviors

$$A_{I,II} \rightarrow (2(1 - C_s^2/C_d^2))^{-1}, \quad B \rightarrow (1 - C_s^2/C_d^2)^{-1}, \quad A_{III} \rightarrow 1, \quad (33)$$

while for high velocities they diverge:

$$A_{I,II} \sim (V_R - V)^{-1}, \quad B \sim (V_R - V)^{-2} \quad (34)$$

when $V \rightarrow V_R$, and

$$A_{III} \sim (C_s - V)^{-1} \quad (35)$$

when $V \rightarrow C_s$. These functions are plotted in Fig. 3.

Equation (26) for $F_1(L, t)$ reproduces the result of Eq. (22): $\vec{V} \cdot \vec{F} = VF_1 = \mathcal{F}$. This result gives a physical interpretation to the material force in the direction of motion of the crack front: it is the component of the force that does work [23,26,30], with the energy needed for that work being supplied by the elastic energy flow into the crack tip. This rela-

tion is well known. Expressions (27) and (28) for the forces F_2 and F_3 however, do not appear to have received much attention in the literature. They are the components of the elastic force perpendicular to the direction of motion, and they do no work. However, they can certainly influence the dynamics of the crack front. Equation (28) shows that there are no tangential forces to the crack edge, i.e., $F_3=0$, a result to be expected in a system that has local two dimensional behavior.

Equation. (27) shows that F_2 depends on the product $K_I K_{II}$ only. This suggests that if an instability mechanism for crack dynamics exists, it will be primarily two dimensional. This is not surprising in view of our assumption of local two dimensionality near the crack tip, and is consistent with the available numerical and experimental evidence. It is important to recall that \mathcal{F} and \vec{F} have been evaluated for a *smooth* crack front $\vec{R}(L,t)$ that propagates at a *smooth* velocity $\vec{V}(L,t) = \partial \vec{R}(L,t) / \partial t$, and also that the curvature of the crack front cannot be very large.

Since $F_2 \neq 0$ if $K_{II} \neq 0$, the direction of the material force acting on the crack front is not necessarily parallel to the direction of crack propagation. The orientation of this force, $\phi(L,t)$, with respect to the normal to the crack front, \vec{e}_1 is given by

$$\tan \phi(L,t) \equiv \frac{F_2}{F_1} = -2C(V) \frac{q}{1+p^2 + \frac{a}{b}q^2}, \quad (36)$$

where

$$q \equiv \frac{b K_{II}}{a K_I}, \quad (37)$$

$$p \equiv \sqrt{\frac{A_{III} K_{III}}{A_I K_I}}, \quad (38)$$

$$C(V) = \frac{2a(1+b^2)(a-b)}{D(V)}. \quad (39)$$

The function $C(V)$ is also universal in the sense that it depends on the local *instantaneous* speed normal to the crack front and on the properties of the material only (see Fig. 4). Its asymptotic behavior is given by

$$C \rightarrow 1 \text{ when } V \rightarrow 0, \quad C \sim (V_R - V)^{-1} \text{ when } V \rightarrow V_R. \quad (40)$$

On the other hand, $\tan \phi$ is an odd function of q . It vanishes when $q \rightarrow \pm \infty$, and it has extrema at $q = \pm \sqrt{(1+p^2)b/a}$.

In the study of crack growth processes in materials which fail in a purely brittle manner, the most commonly used crack growth criterion is the generalization of Griffith's critical energy release rate criterion [8,20]. According to the generalized Griffith criterion, the crack must grow in such a way that G is always equal to a newly defined quantity: the dynamic fracture energy of the material, Γ . The growth criterion is [8]

$$G = \Gamma. \quad (41)$$

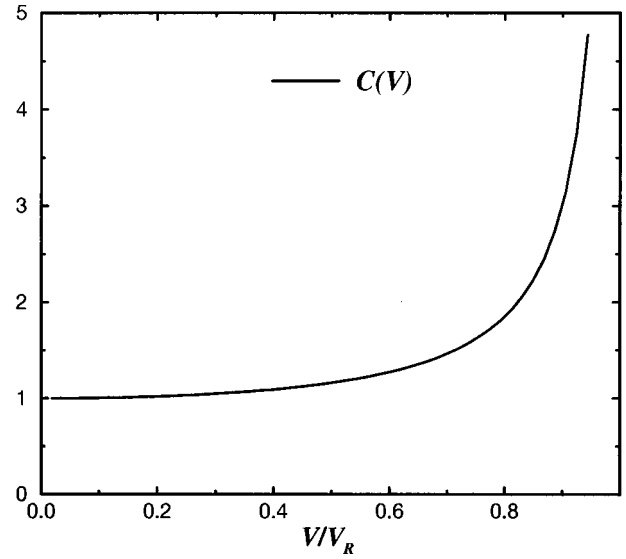


FIG. 4. Universal function $C(V)$, given by Eq. (39), plotted as a function of V/V_R for $C_d = \sqrt{3}C_s$.

This relation is called an equation of motion for the crack front. The energy release rate G is a property of the local mechanical fields. The dynamic fracture energy Γ , on the other hand, represents the resistance of the material to crack advance; it is assumed to be a property of the material determined by the energy needed to create new crack surface, including whatever nonlinear microscopic processes take place very near the crack tip. Its value can be determined only through laboratory measurements, or, eventually, by way of microscopic models.

On the other hand, Eqs. (25) and (26) show that the energy release rate G is equivalent, in Eshelby's approach, to a force per unit length of the crack front. Equation (41) can be reinterpreted as a balance between the component F_1 of the material force along the direction of motion, and a resistance force to crack advance per unit length of the crack front: $F_1 = \Gamma$. As stated in Sec. I, one equation of motion is not enough to determine the trajectory of a crack that is allowed to deviate from straight line motion. A popular additional requirement to determine a crack trajectory in two dimensions is the principle of local symmetry [21,22]:

$$K_{II} = 0 \quad \Leftrightarrow \quad (\text{smooth crack propagation}); \quad (42)$$

that is, that propagation without branching occurs in such a way as to keep a purely opening mode at the crack tip. This principle has been essentially developed for quasistatic regimes [22] (see also Ref. [33] for a discussion), although it has also been used in the dynamic case [34].

The fact that the usual energy criterion used to determine crack evolution can be interpreted as one component of a balance of forces suggests a different approach: Why not use a balance of forces criterion for all three components? This would give the requisite number of equations needed to determine the evolution of a crack front. In Sec. V, we shall develop this idea, in which the principle of local symmetry is not assumed to hold *a priori*.

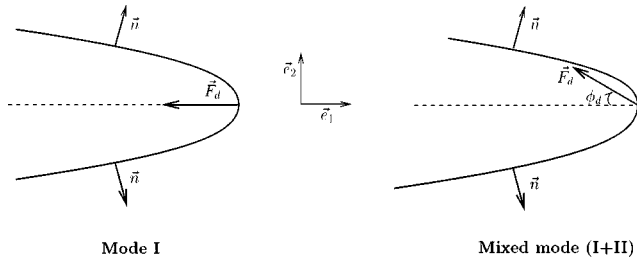


FIG. 5. A simple model of the “shape” of newly created surface in the vicinity of the crack tip and the associated forces of surface tension. Pure tension gives a symmetric opening. Mixed mode loading breaks this symmetry.

V. A MODEL FOR AN EQUATION OF MOTION OF THE CRACK FRONT

So far, we have determined the material forces [Eqs. (26), (27), and (28)] acting on the crack front. In order to write down an equation of motion, we will assume that these material forces are exactly balanced by dissipative forces of microscopic origin acting within the crack front region. These new forces represent the resistance of the material to crack advance. Our task is now to advance a model for these forces that will allow mathematical analysis to be performed.

Here we introduce a simple two-dimensional model of what happens within the crack front region in order to obtain some insight into the physics of the forces acting at the crack front. Our purpose is to obtain qualitative understanding, and not necessarily to provide an accurate picture of the microphysics near the crack tip. Suppose that the crack tip, even at very small scales, can be described by a continuous curve Σ of high curvature (see Fig. 5). In reality, this surface is not well defined. We assume, nevertheless, there exists an energy U associated with the creation of *curved* surface at the crack front. That is,

$$U = \gamma \int_{\Sigma} dS, \quad (43)$$

with dS an element of crack surface and γ a surface tension that will be assumed constant for simplicity. This means that U is proportional to the amount of new surface created, a reasoning that is closely analogous to the original approach of Griffith [20], who associated the energy released during crack growth to the energy required to create a unit of new surface area. If the surface of the crack is changed by displacing each element by an amount $\delta\vec{X}$, the change in the surface energy U of Eq. (43) is

$$\delta U = -\gamma \int_{\Sigma} dS \frac{\hat{n} \cdot \delta\vec{X}}{R}, \quad (44)$$

where \hat{n} is the unit vector normal to the surface that points into the material, and R is the radius of curvature at each point of the original surface (it is negative if the curvature is measured with respect to a point outside the material). This allows us to identify

$$\vec{F}_d = \gamma \int_{\Sigma} dS \frac{\vec{n}}{R} \quad (45)$$

as the force originating from surface tension, that would balance the material forces in this simple model.

The implication of this simple model for mode I loading is (see Fig. 5) that the contribution to the resistance force of the upward and downward surfaces near the tip are symmetric, and thus

$$\vec{F}_d \approx -\gamma \int_{-\theta_0}^{\theta_0} d\theta (\cos \theta \vec{e}_1 + \sin \theta \vec{e}_2) = -\Gamma \vec{e}_1, \quad (46)$$

where θ is the angle between the normal to the surface and the direction \vec{e}_1 . In Eq. (46), we have used the equality $dS = R d\theta$. The magnitude of the dissipative force F_d is adjusted to the value already mentioned in Eq. (41), with $\Gamma \approx 2\gamma \sin \theta_0$ and, for symmetry reasons, it points along the direction of motion.

In the presence of mode II loading, reflection symmetry with respect to the direction of motion is broken. We write then the resistance force in the mixed mode case as

$$\begin{aligned} \vec{F}_d &\approx -\gamma \int_{-\theta_0 + \phi_d}^{\theta_0 + \phi_d} d\theta (\cos \theta \vec{e}_1 + \sin \theta \vec{e}_2) \\ &= -\Gamma (\cos \phi_d \vec{e}_1 + \sin \phi_d \vec{e}_2), \end{aligned} \quad (47)$$

with ϕ_d an angle yet to be modeled. This angle takes into account the asymmetric contributions to the resistance force of the upward and downward surfaces near the tip. The direction of resistance forces is not necessarily parallel to the direction of motion. The general idea of this simple model is that the curvature created will adjust itself so as to balance the material forces acting at the tip. This hypothesis of existence of a perpendicular resistance force is reminiscent of the approaches used to generalize cohesive zone models in the presence of shear [13], or to model fracture energy of interface cracks [35].

From now on, leaving aside the specifics of the simple model just presented, we will assume that these resistance balancing forces do exist, and that they have the form suggested by Eq. (47):

$$\vec{F}_d = -\Gamma (\cos \phi_d \vec{e}_1 + \sin \phi_d \vec{e}_2). \quad (48)$$

Also, we assume that the angle ϕ_d , that defines the direction of the resistance force, is a function of q , or K_{II}/K_I , the relative amount of local shear with respect to local tensile loading, and of crack velocity V , which are parameters of the forcing. For an isotropic body, it is clear that ϕ_d should be an odd function of K_{II} in order to respect the symmetry of mode II. Therefore, without loss of generality, the tangent of the angle of the crack tip force will be written as

$$\tan \phi_d = -2\alpha(V)q\psi(q, V), \quad (49)$$

where $\psi(q, V)$ is an undetermined even function of q , and $\psi(0, V) = 1$. When K_{II} is small compared to K_I we can expand the function ψ for small q :

$$\psi(q, V) = 1 + \beta(V)q^2 + \dots \quad (50)$$

We will assume $\beta(V) \geq 0$ for reasons to be explained in Sec. VI. Furthermore, $\tan \phi_d$ has been written in a suggestive

form, introducing a velocity dependent factor $\alpha(V)$ that is a local measure, at the crack front, of the competition between shear and opening, and it should be related to the micromechanics at the crack tip. The precise nature of this relation, however, is outside the scope of the present work.

A simple estimate of the order of magnitude of the parameter $\alpha(V)$ can be obtained in the quasistatic limit, by comparison with a crack having a kink. In this case evaluating Eq. (36) for $V=0$ shows that the orientation of the material force with respect to the normal to the crack front becomes $\phi \approx -2q$ for $q \ll 1$. On the other hand, in the presence of mode II loading, the principle of local symmetry (42) implies that a crack that is at a critical value of incipient growth will branch locally in a direction ϕ_B that satisfies a pure opening mode at the crack tip. When $q \ll 1$, this direction is also given by $\phi_B \approx -2q$ [33]. We take this fact as an indication that, for small velocities we shall also have $\phi_d \approx -2q$, so that

$$\alpha(0) \approx 1. \quad (51)$$

On this basis we shall take $\alpha(V)$ to be a positive function of V and of order one at low velocities.

Finally, Eqs. (26), (27), and (48) allow us to write down a set of two dynamic equations of motion on the following basis: since the usual Griffith criterion [Eq. (41)] can be interpreted as a balance of one component of the forces acting at the crack tip, we extend this requirement to hold for *both* force components: elastodynamic force must be exactly balanced by dissipative force at the crack front. That is,

$$\tan \phi_d = \tan \phi = -2C(V) \frac{q}{1 + p^2 + \frac{a}{b} q^2}, \quad (52)$$

$$\Gamma \cos \phi_d = F_1 = \frac{1}{2\mu} \left(1 + p^2 + \frac{a}{b} q^2 \right) A_I(V) K_I^2. \quad (53)$$

Our assumption, implicit in Eq. (49), that material parameters depend on velocity but not on higher order time derivatives of crack tip position, implies that the crack tip has no inertia.

VI. SOLUTIONS TO THE EQUATION OF MOTION

In this section we consider the case $K_{III}=0$, i.e., $p=0$. The case $p \neq 0$ will be discussed qualitatively in Sec. VII.

If we introduce Eq. (49) into Eq. (52), we obtain

$$-2\alpha(V)q\psi(q,V) = -2C(V) \frac{q}{1 + \frac{a}{b} q^2}. \quad (54)$$

Equation (54) is a local equality between the angles of the material forces and the resistance forces with the direction of crack propagation. It can be solved for q , independently of the specific loading conditions and geometry. $q=0$ is always a solution to Eq. (54) (see Fig. 6). We will also assume that $\alpha(V)$ is a slowly varying function of V compared with the variation of $C(V)$. This allows the number of solutions of Eq. (54) to be determined by the magnitude of the slope of the right and left hand sides at $q=0$. These slopes are equal

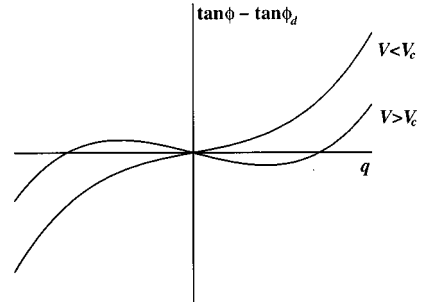


FIG. 6. Graphic solution of Eq. (54) for different values of V . The critical velocity V_c is determined by condition (55).

to $2\alpha(V)$ and $2C(V)$, respectively. Since $C(V)$ is an increasing function of velocity V with $C(0)=1$ (Fig. 4), the condition that slopes be equal at $q=0$ leads to the conclusion that, for $\alpha \geq 1$ and $\beta(V) \geq 0$ there exists a critical velocity V_c for which

$$C(V_c) = \alpha(V_c), \quad (55)$$

below which, i.e., for $V < V_c$, $K_{II}=0$ is the only solution to Eq. (54) while for $V > V_c$ there are three solutions, $K_{II}=0$ and $K_{II} = \pm g(V)K_I$ (Fig. 7),

$$V < V_c \Leftrightarrow \alpha(V) > C(V) \Leftrightarrow K_{II}=0, \quad (56)$$

$$V > V_c \Leftrightarrow \alpha(V) < C(V) \Leftrightarrow K_{II}=0, \quad K_{II} = \pm g(V)K_I. \quad (57)$$

The function $g(V)$ can be computed only if the function $\psi(q,V)$ is known. Even in the vicinity of V_c one needs to know the coefficient $\beta(V)$, in order to compute $g(V)$. However, it can be determined that for velocities V just above V_c , the function $g(V)$ behaves as $(V/V_c - 1)^{1/2}$. This results from solving Eq. (54), with both sides written to order q^3 . As seen in Fig. 7, the velocity V acts as a bifurcation parameter at $V=V_c$ for the solutions of Eq. (54) as a function of q , or K_{II}/K_I . As V grows over V_c , the new solutions with $K_{II} \neq 0$ are increasing functions of V , away from $K_{II}=0$ at $V=V_c$. This is a signature of a second order transition. If $\alpha(V) < 1$, there would always exist three solutions to our equation [since $C(V) \geq 1$], and the above transition would be absent. Notice also that the critical velocity V_c always satisfies $V_c < V_R$, since $C(V) \rightarrow \infty$ as $V \rightarrow V_R$.

Given different solutions to the equation of motion for $V > V_c$, the question arises of what is the selection mechanism that will decide which possibility will be chosen by a

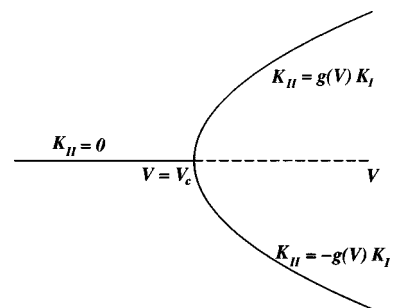


FIG. 7. Schematic phase diagram of the solutions $K_{II}(V)$ of Eq. (54), showing the second order transition.

traveling crack. Consider a first configuration of *smooth* crack propagation at an instantaneous velocity $V > V_c$, with stress intensity factors $K_I \neq 0$ and $K_{II} = 0$. From Eqs. (25), (52), and (53), the rate of energy flow needed for the propagation of this crack is

$$\mathcal{F} = V\Gamma. \quad (58)$$

Consider a second configuration of *smooth* crack propagation with the same instantaneous velocity V , but with stress intensity factors satisfying $K_I \neq 0$ and $K_{II} = \pm g(V)K_I$. From Eqs. (25) and (53), the rate of energy flow needed for the propagation of this crack is

$$\mathcal{F}' = V\Gamma \cos \phi_d. \quad (59)$$

Clearly, $\mathcal{F}' \leq \mathcal{F}$: the material response to external loading provides less energy per unit time for the second configuration than for the first one. Above the critical velocity, the crack needs more energy to advance in a configuration at the state $K_{II} = 0$ with a velocity V than in the one at the state $K_{II} \neq 0$ with the same velocity V . Therefore, above V_c , the crack propagation selects one of the solutions $K_{II} = \pm g(V)K_I$, instead of the solution $K_{II} = 0$. Consequently, when the crack tip velocity is below V_c , the crack propagation satisfies the principle of local symmetry [Eq. (42)]. However, for $V > V_c$, this principle no longer holds, and the crack propagation with a pure opening mode at the tip becomes unstable with respect to solutions satisfying $K_{II} = \pm g(V)K_I$ (see Fig. 7).

To summarize, we have shown that, subject to conditions explained in detail above, there is a critical velocity at which the dynamics of a crack undergoes a transition from being determined by $K_{II} = 0$ to being determined by $K_{II} \neq 0$. The trajectory itself, however, remains smooth with smoothly turning tangents. Note that nowhere in the last two sections have we made any assumption concerning a possible dependence of the fracture energy of the material Γ upon velocity.

VII. SCENARIO RELATED TO EXPERIMENTAL RESULTS

In this section we use our model to attempt an explanation of some features of the experimental results in fast fracture under mode I loading of thin plates of glass and plexiglass [1–5]. These experiments show a dynamic instability at a critical velocity that is about a third of the Rayleigh velocity of the material. This instability is associated with the roughening of the crack surfaces, the appearance of microcracks, crack tip velocity oscillations, and strong acoustic emissions. We wish to explore the consequences of identifying the critical velocity V_c of our model with the experimental critical velocity. Using $C_d \approx \sqrt{3}C_s$, and from Eqs. (39) and (55), this value can be obtained with $\alpha(V_c) \approx 1.073$, which is a reasonable value according to the estimates of Sec. V.

A. Low velocities, $V < V_c$

In this case, the only possible solution is $K_{II} = 0$. From Eq. (53), and assuming $K_{III} = 0$, one recovers the well known equation of motion [8]

$$\frac{1}{2\mu}A_I(V)K_I^2 = \Gamma, \quad (60)$$

which determines the crack tip velocity. The result $K_{II} = 0$ means that the crack will propagate following a smooth path, with a pure opening mode at the tip. This is the statement of the principle of local symmetry [Eq. (42)]. Our approach can be regarded as a derivation and an extension of this principle to nonzero velocities $V < V_c$.

This solution corresponds then to the experimentally observed mirror region, where the crack propagation follows a straight path. For a crack under uniaxial loading, this corresponds to the direction that satisfies $K_{II} = 0$ during the crack propagation. Since this path appears to be stable, we expect that small perturbations away from this straight line propagation will be damped away [36].

B. High velocities, $V > V_c$

As the velocity of the crack surpasses V_c , the propagation satisfying $K_{II} = 0$ at the crack tip becomes unstable. The crack now propagates in one of the two new directions satisfying $K_{II} = \pm g(V)K_I$. It is important to notice that the allowed values of K_{II}/K_I grow continuously with V from 0 at $V = V_c$, and that these new solutions correspond to *smooth* crack propagation.

Experiments show that at velocities higher than a critical value the surface left behind after rupture becomes rough, and microcracks appear. As we have noted, an experiment carried out in pure tension leads to a straight path in the case $K_{II} = 0$. The solution $K_{II} = \pm g(V)K_I \neq 0$ means then that the trajectory of the crack tip will deviate from a straight line. Smooth crack propagation with $K_{II} \neq 0$ explains the observed appearance of microcracks, because on the crack faces the stress components p_{22} and p_{12} vanish identically. However, in the presence of a shear mode at the crack tip, it is seen from Eq. (23) that the near field asymptotic stress p_{11} at the moving crack tip is singular on the crack faces [8]:

$$p_{11}(r, \pm \pi) \sim \mp K_{II}/\sqrt{r}. \quad (61)$$

This means that there is a high tensile stress near the tip that, if given the chance, will tend to open microcracks on one of the crack faces in a direction that is initially perpendicular to the direction of motion of the main crack. Small perturbations may thus initiate microcracks that will start perpendicularly to the main crack, and later on will deviate into a direction closer to the direction of motion of the main crack, in order to avoid the unloaded region which is left behind the crack tip. Also, the formation of these microcracks may tend to slow down the main crack due to the expenditure of energy on surface creation [4]. As this happens the ratio K_{II}/K_I will decrease, leading to a trajectory change back toward the initial crack trajectory. This may be the reason for the appearance of bumps on the crack surfaces (see Fig. 8). This description of the microbranching process does not require any discontinuity in the velocity of the main crack.

C. Presence of a mode III

Equations (49) and (52) suggest that the presence of non-vanishing mode III loading may be taken into account within

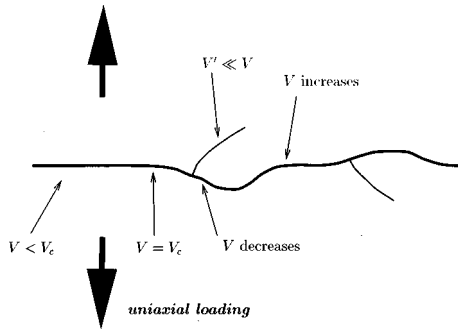


FIG. 8. Scenario for the trajectory of a crack submitted to uniaxial loading. At low velocities there is straight line propagation (mirror zone). Above the critical velocity the trajectory deviates from a straight line. $K_{II} \neq 0$ allows for microcracks to sprout behind the advancing crack tip. Their energy expenditure slows down the main crack, possibly below the critical velocity. This would reorient the crack back to straight line propagation.

the $K_{III} = 0$ arguments simply by replacing the parameter α by a modified “effective” value α_{eff} ,

$$\alpha_{\text{eff}}(V) = (1 + p^2)\alpha(V), \quad (62)$$

that will now determine the value of the critical velocity. Thus the presence of an out of plane mode has a stabilizing effect, in the sense that the value of the critical velocity V_c for the instability to appear is increased. In other words, the instability will appear first at points on the crack front where K_{III} vanishes. This provides a rationale to understand the experimental fact [4] that microcracks first appear near the edges of the plate. Indeed, we do expect the crack front to deviate from a straight line perpendicular to both faces of the plate. Consequently, in general, we shall have $K_{III} \neq 0$ except near the faces of the plate where the condition $K_{III} = 0$ will be enforced by the free surface condition $p_{ij}n_j = 0$. Therefore, the minimal value of α_{eff} will be at the faces of the plate, and that is where the instability will start. As the mean crack velocity increases, the roughness and microbranches increase, because more and more points on the crack front reach the critical velocity. This explains why roughness and microcrack penetration increases with increasing velocity [4].

VIII. CONCLUSION

We have developed an approach to crack dynamics based on the balance of energy and field momentum for a moving crack in three dimensions [26,30]. We have derived the energy flow rate into the crack front and the configurational forces acting on it. The components of the material force at the crack front have been computed in the framework of the linear isotropic elastodynamic model. It has been found that the orientation of this force is not necessarily in the direction of crack propagation. Within a Griffith-like approach, we have defined a generalized dissipative force at the crack front. Assuming that this dissipative force exactly balances the material force at the crack front, we derived a vector equation of motion for the crack front. Under minimal assumptions, we have shown that there exists a critical velocity below which a crack propagates in a direction that keeps a pure opening mode at the tip. At the critical velocity there is a second order dynamic instability, and above the critical velocity the crack growth with a pure opening mode at the tip becomes unstable with respect to two new possible solutions. Various experimental manifestations have been described qualitatively under the light of this model.

Our approach is universal in the sense that the instability mechanism we have presented is local at the crack tip, and it is independent of the specific loading configuration and the geometry of the experiment. It will hold for any isotropic elastic material. Throughout the analysis, it has not been specified that the configuration of the pure opening mode of the crack tip has to be a straight path. Such a configuration could be a curved path, but the instability we have discussed would still occur. The instability mechanism originates in a balance between forces of elastic origin and material dissipative forces of microscopic origin which have been modeled. A detailed microscopic justification of this modeling suggests itself as an interesting avenue for future research.

ACKNOWLEDGMENTS

M.A.-B. is grateful to Professor J.R. Rice for helpful discussions and critical comments. R.A. and F.L. gratefully acknowledge the support of a Cátedra Presidencial en Ciencias. This collaboration was made possible by a grant from CNRS, Conicyt, and Fondecyt Grant No. 1960892. Laboratoire de Physique Statistique is associated with the CNRS (UMR 8550) and Universities Paris VI and Paris VII.

- [1] J. Fineberg, S.P. Gross, M. Marder, and H.L. Swinney, Phys. Rev. Lett. **67**, 457 (1991); Phys. Rev. B **45**, 5146 (1992).
- [2] S.P. Gross, J. Fineberg, M. Marder, W.D. McCormick, and H.L. Swinney, Phys. Rev. Lett. **71**, 3162 (1993).
- [3] E. Sharon, S.P. Gross, and J. Fineberg, Phys. Rev. Lett. **74**, 5096 (1995); **76**, 2117 (1996).
- [4] E. Sharon and J. Fineberg, Phys. Rev. B **54**, 7128 (1996).
- [5] J.F. Boudet, S. Ciliberto, and V. Steinberg, Europhys. Lett. **30**, 337 (1995); J. Phys. II **6**, 1493 (1996).
- [6] K. Ravi-Chandar and B. Yang, J. Mech. Phys. Solids **45**, 535 (1997).
- [7] J.F. Boudet and S. Ciliberto, Phys. Rev. Lett. **80**, 341 (1998).
- [8] L.B. Freund, *Dynamic Fracture Mechanics* (Cambridge University Press, Cambridge, 1990).
- [9] W.G. Knauss and K. Ravi-Chandar, Int. J. Fract. **27**, 127 (1985).
- [10] J. R. Rice, Y. Ben-Zion, and K.-S. Kim, J. Mech. Phys. Solids **42**, 813 (1994).
- [11] F. Lund, Phys. Rev. Lett. **76**, 2742 (1996).
- [12] H. Gao, J. Mech. Phys. Solids **41**, 457 (1993); **44**, 1453 (1996); Philos. Mag. Lett. **76**, 307 (1997).
- [13] E.S.C. Ching, J.S. Langer, and H. Nakanishi, Phys. Rev. E **53**, 2864 (1996).
- [14] J.S. Langer and A.E. Lobkowsky, J. Mech. Phys. Solids **46**, 1521 (1998).
- [15] M. Marder and S.P. Gross, J. Mech. Phys. Solids **43**, 1 (1995).
- [16] X.P. Xu and A. Needleman, J. Mech. Phys. Solids **42**, 1397 (1994).

- [17] F.F. Abraham, D. Brodbeck, R.A. Rafey, and W.E. Rudge, Phys. Rev. Lett. **73**, 272 (1994).
- [18] S.J. Zhou, P.S. Lomdahl, R. Thomson, and B.L. Holian, Phys. Rev. Lett. **76**, 2318 (1996).
- [19] P. Gumbsch, S.J. Zhou, and B.L. Holian, Phys. Rev. B **55**, 3445 (1997).
- [20] A.A. Griffith, Philos. Trans. R. Soc. London, Ser. A **221**, 163 (1920).
- [21] R.V. Gol'dstein and R.L. Salganik, Int. J. Fract. **10**, 507 (1974).
- [22] M. Amestoy and J.B. Leblond, C. R. Acad. Sci., Ser. II: Mec. Phys., Chim., Sci. Terre Univers **301**, 969 (1985).
- [23] J.R. Rice, J. Appl. Mech. **35**, 379 (1968).
- [24] B.V. Kostrov and L.V. Nitkin, Arch. Mech. Stosow. **22**, 749 (1970).
- [25] J.D. Eshelby, Philos. Mag. **42**, 1401 (1951).
- [26] J.D. Eshelby, in *Inelastic Behavior of Solids*, edited by M. F. Kanninen, W.F. Adler, A.R. Rosenfield, and R.I. Jaffee (McGraw-Hill, New York, 1970), p. 77.
- [27] M.E. Gurtin and P. Podio-Guidugli, J. Mech. Phys. Solids **44**, 905 (1996); **46**, 1343 (1998).
- [28] M.E. Gurtin and M.M. Shvartsman, J. Elast. **48**, 167 (1997).
- [29] M. Adda-Bedia, R. Arias, M. Ben Amar, and F. Lund, Phys. Rev. Lett. **82**, 2314 (1999).
- [30] G.A. Maugin, Acta Mech. **105**, 33 (1994).
- [31] We have, however, considered curves C , whose end points coincide, i.e., they are on exactly opposite sides of the crack surface. The question naturally arises as to what happens if this is not the case. This is a subtle question. Let the length of the curve be of order ϵ , a quantity small compared to any length scale relevant to the problem such as crack length or acoustic wavelength. For a smooth curve, ϵ will also be the order of magnitude of the distance between points on the curve and crack tip. Now let δ be the nonzero distance, measured along the crack surface, between the beginning and end of C . If δ is of order smaller than order ϵ , the contribution from this extra surface vanishes, and the independence of Eqs. (15) and (16) from the integration path still holds. If δ is of order ϵ or larger, it does not. What this means is that the dynamical variable whose equation of motion we are trying to find is actually a small region enclosed within a smooth boundary that encircles the crack tip, whose end points are not very far from each other. This is our operational definition of "crack tip."
- [32] R. Dmowska and J.R. Rice, in *Continuum Theories in Solid Earth Physics*, edited by R. Teisseyre, Physics and Evolution of the Earth's Interior Vol. 3 (Elsevier, Amsterdam, 1986), p. 187.
- [33] B. Cotterell and J. Rice, Int. J. Fract. **16**, 155 (1980).
- [34] M. Adda-Bedia, M. Ben Amar, and Y. Pomeau, Phys. Rev. E **54**, 5774 (1996).
- [35] A.G. Evans, M. Rühle, B.J. Dalgleish, and P.G. Charalambides, Mater. Sci. Eng., A **126**, 53 (1990).
- [36] For a discussion of the stability of straight line crack motion within the context of thermal fracture, see M. Adda-Bedia and Y. Pomeau, Phys. Rev. E **52**, 4105 (1995).